Molecular adsorption on oxide surfaces: Electronic structure and orientation of NO on NiO(100)/Ni(100) and on NiO(100) as determined from electron spectroscopies and *ab initio* cluster calculations

H. Kuhlenbeck, G. Odörfer, R. Jaeger, G. Illing, M. Menges, Th. Mull, and H.-J. Freund
Lehrstuhl für Physikalische Chemie I, Ruhr-Universität Bochum, Universitätsstrasse 150, D-4630 Bochum, Federal Republic of Germany

M. Pöhlchen and V. Staemmler
Lehrstuhl für Theoretische Chemie, Ruhr-Universität Bochum, Universitätsstrasse 150, D-4630 Bochum, Federal Republic of Germany

S. Witzel, C. Scharfschwerdt, K. Wennemann, T. Liedtke, and M. Neumann
Fachbereich Physik, Universität Osnabrück, Barbarastrasse 7, D-4500 Osnabrück, Federal Republic of Germany
(Received 30 July 1990)

We have investigated the adsorption of NO on a thin NiO(100) film of several layers thickness grown on top of a Ni(100) surface in comparison with data of an *in vacuo* cleaved NiO(100) single crystal. The layer exhibits a high defect density. We demonstrate via application of several surface-sensitive electron-spectroscopic techniques [i.e., x-ray photoelectron spectroscopy (XPS), angle-resolved ultraviolet photoelectron spectroscopy (ARUPS), near-edge x-ray-absorption fine structure (NEXAFS), and high-resolution electron-energy-loss spectroscopy (HREELS)] that this layer has similar occupied (ARUPS) and unoccupied (NEXAFS) states as a bulk NiO(100) sample. In spite of its limited thickness, the band structure of the film exhibits dispersions perpendicular to the surface compatible with bulk NiO(100). It is shown that the electronic structure of the oxygen sublattice can be described in a band-structure picture while for the Ni sublattice electron localization effects lead to a breakdown of the band-structure picture. NO on NiO desorbs at 220 K. This indicates weak chemisorption. The NO coverage is close to 0.2 relative to the number of Ni surface atoms as determined by XPS. HREELS reveals that there is only one species on the surface documented by the observation of only one bond-stretching frequency. NEXAFS data on the system and a comparison with previous data on the system NO/Ni(100) indicate that the molecular axis of adsorbed NO is tilted by an angle of approximately 45° relative to the surface normal. The N 1*s* XP spectra of the weakly chemisorbed species show giant satellites similar to the previously observed cases for weak chemisorption on metal surfaces. This is the first observation of an intense satellite structure for an adsorbate on an insulator surface, which shows that there must be sufficient screening channels even on an insulating surface. A theoretical assignment of the peaks is discussed. We compare the spectroscopic properties of the NO species on the thin-film oxide surface, which is likely to contain a certain number of defects, with NO adsorbed on a basically defect-free bulk oxide surface by thermal-desorption (TDS) and XP spectra. TDS and XP spectra of the bulk system are basically identical as compared with the oxide film, indicating that the majority of species adsorbed on the film is not adsorbed on defects but rather on regular NiO sites. Results of *ab initio* oxide cluster calculations are used to explain the bonding geometry of NO on regular NiO sites.

I. INTRODUCTION

Metal oxides, and transition-metal oxides in particular, are in use as catalysts in industrial processes. This is certainly one of the reasons why the study of adsorption and reaction on oxide surfaces has been pioneered rather early in the fifties and sixties. With the advent of surface science the interest has shifted towards clean metal surfaces and the study of metal oxides has been abandoned to some extent. During the last decade or so, however, the interest in oxide surfaces has been revitalized and some clean single-crystal surfaces have been studied by applying surface-science methodology. Henrich has recently published an excellent review of this field.[1] For certain oxides, i.e., semiconducting oxides such as ZnO, a great deal of information already exists even for molecular adsorbates on these surfaces. Much of this literature has been collected in a review by Heiland and Lüth.[2] It appears, though, that ZnO is a singular case. One issue has been that many oxides exhibit only limited conductivity which in turn limits the applicability of electron-spectroscopic techniques which play a central role in the characterization of clean surfaces and of molecular adsorbates on these surfaces. Some of the latter difficulties may be circumvented by looking at thin oxide films grown on metallic substrates. In certain cases such oxide

films are ordered and may be characterized via low-energy electron diffraction (LEED). These films are then ideally suited to study molecular adsorption via electron spectroscopy because their conductivity is sufficiently high and the surface-science machinery may be applied. A review on the oxidation of metal surfaces has been published by Wandelt.[3]

One such case is NiO where it is well known that on Ni(100) and on Ni(111) faces rather well-ordered NiO surfaces in (100) and (111) orientations may be grown.[4,5] These films are known to have a thickness of three to four monolayers and exhibit a limited number of defects.[6] We have investigated the structure of these films with scanning tunneling-microscopy (STM) and spot profile analysis of LEED (SPA-LEED). The results of this study will be published elsewhere.[7]

Several electron-spectroscopic investigations have been performed so far on clean "well-ordered" films[8–13] and we shall refer to them in the course of this paper, but molecular adsorption has been preferentially studied on NiO powders[14] although there are some studies on single crystals[15,16] and thin films.[17–22] Briefly, it is generally believed that in catalytic oxidation reactions adsorption of diatomic molecules only takes place on those parts of the polycrystalline surfaces that contain cationic vacancies, i.e., on NiO substrates that are oxygen enriched.[23] The cationic vacancies are believed to lead either to the formation of Ni^{3+} centers which act as adsorption sites for oxidation and/or to the formation of O^- centers which react with incoming molecules.[23]

In order to study the influence of defects in a controlled fashion, we begin our investigations with a detailed study of clean and NO-covered bulk NiO(100) and NiO(100) films grown on Ni(100). We determine the electronic band structure of the clean film and compare it with the band structure of bulk NiO, applying angle-resolved ultraviolet photoelectron spectroscopy (ARUPS). This is done to ensure that when we study NO adsorption on films we know about deviations from the bulk electronic properties due to the finite thickness and stoichometry of the NiO film. By comparing the adsorption behavior of the film and the bulk crystal we have the unique opportunity to directly study the influence of defects on the adsorption of molecules because the thin films exhibit a much higher defect density as revealed by electron-energy-loss spectroscopy (HREELS), x-ray photoelectron spectroscopy (XPS), near-edge x-ray-absorption fine structure (NEXAFS), and thermal-desorption spectroscopy (TDS). It is found that NO is weakly chemisorbed and bound nitrogen end down on top of a nickel site with its molecular axis tilted with respect to the surface normal. Comparison with thermal-desorption data of NO on bulk NiO, which is known to exhibit a much lower defect density on the surface than the film, convince us that adsorption takes place primarily on nondefect, regular, NiO sites.

II. EXPERIMENTAL DETAILS

The experiments were performed in several different ultrahigh-vacuum (UHV) systems. NEXAFS and ARUPS data were recorded using synchrotron radiation from the storage ring BESSY (Berliner Elektronenspeicherring-Gesellschaft für Synchrotronstrahlung mbH) in Berlin, Germany, and the HASYLAB synchrotron radiation center in Hamburg, Germany. The HREELS data have been taken in a UHV system equipped with a Leybold ELS22 system with a typical resolution of 8 meV. XPS data of the film were taken in a UHV system equipped with an VSW (Vacuum Science Workshop) x-ray gun and a 10-cm VSW spherical electron-energy analyzer, whereas the XPS data of the bulk sample were recorded in a VG Instruments ADES400 system equipped with a Perkin-Elmer x-ray tube using a rotable analyzer. In addition, TDS spectra could be taken and LEED and Auger electron spectroscopy (AES) analysis were performed to check the cleanliness of the crystal.

The Ni(100) sample was spot welded to two tungsten rods which were connected to a liquid-nitrogen reservoir such that the sample could be cooled below 100 K, and heated by electron bombardment of the reverse side of the crystal. The surface was prepared by repeated cycles of Ne-ion etching and heating to 800 K.

The NiO(100) sample was attached to a tantalum foil which was mounted to a standard VG sample holder and could be cleaved *in vacuo*. Photon energy was calibrated with use of a gold foil mounted near the sample.

The NEXAF spectra were recorded by monitoring the nitrogen and oxygen K-edge Auger yields in a 12-eV-wide window centered at 511 and 380 eV, respectively, as a function of photon energy. NEXAF spectra presented here are difference spectra and have been normalized to the absorption step height as was done previously.[24]

III. RESULTS AND DISCUSSION

A. Clean NiO(100)/Ni(100) and NiO(100)

1. XPS data

In Fig. 1 we show O 1s and Ni $2p_{1/2,3/2}$ spectra of the surface taken during preparation of the NiO(100) surface. On the left-hand side of the figure we have included photographs of the observed LEED structures. For the clean surface we find the typical (100)1×1 pattern. The Ni 2p spectra exhibit the well-known shape, i.e., a strong main line due to the configuration $2p^5 3d^{10}$ together with the famous 6-eV satellite due to the configuration $2p^5 3d^9 4s^1$.[25–27] After exposure of oxygen at room temperature we observe consecutively $p(2\times2)$ and $c(2\times2)$ patterns.[28,29] The latter is shown together with the corresponding x-ray photoelectron (XP) spectra. A slightly asymmetric O 1s feature is observed, typical for an atomic adsorbate on a metallic substrate. The Ni 2p levels are basically unchanged except for an increase in linewidth and concommitantly an increase of intensity in the region between the satellite and main line. Upon further increase of oxygen exposure we recognize a hexagonal LEED pattern which has been called in the past a NiO(111) pattern.[28] This point shall not be addressed any further in this paper. We realize, however, that the XP spectra indicate differences as well from the O 1s and Ni 2p spectra of the oxygen adsorbate as from the NiO(100) spectra which will be addressed in the following. Repeat-

ed cycles of dosing 1000 L O_2 (1 L$=10^{-6}$ Torr sec) at $T=570$ K and subsequent annealing to $T=650$ K resulted in a LEED pattern characteristic for a NiO sample exposing the (100) surface to the vacuum. The larger lattice constant of NiO as compared with metallic Ni manifests itself in a smaller spot separation in the LEED pattern. Obviously, the NiO(100) surface must contain a number of defects because the spots are considerably more diffuse as compared with the surface of a vacuum-cleaved bulk NiO sample which exhibits the same but very sharp LEED spots as shown in the top LEED pattern. The XP spectra of the thin oxide film are shifted to a higher binding energy as compared to the spectra of the cleaved oxide. This is due to a shift of the Fermi level which is determined by the defect states and will be discussed in the following section. The nature of these defects is widely unknown and will be addressed in a forthcoming paper.[7] One hint as to whether these defects are connected with the nonstoichiometry of the thin film can be gained from the intensity ratios I_{Ni}/I_O of the bulk and the film sample. While the bulk sample exhibits a more or less perfect 1:1 stoichiometry the film shows a 0.8:1 ratio implying higher oxygen content. Whether this points towards Ni vacancies, known to be the dominant defect in the bulk,[30] is still unclear, but high resolution LEED and STM studies are in progress.[7] We shall show in Sec. III B that these defects do not seem to determine the adsorption behavior of the NiO(100) surface with respect to NO. For this NiO(100) surface we observe a Ni $2p$ spectrum which is now quite different from the spectra discussed before. Each of the two principal components of the Ni $2p_{1/2,3/2}$ is dominated by at least three features which are considerably shifted with respect to the spectra of the metallic surfaces. On the other hand, we see one strong, more or less symmetric O $1s$ feature with a binding energy of 530.2 eV with respect to the Fermi level of the metallic Ni substrate, which is only marginally different from the O $1s$ spectra measured on the previously discussed systems. Without any further detailed assignment at this point (however, see below) we can proceed to a rather important conclusion: It is the Ni rather than the oxygen which experiences considerable changes in its electronic structure when going from O/Ni(100) to NiO(100). This is quite in accord with expectations if we

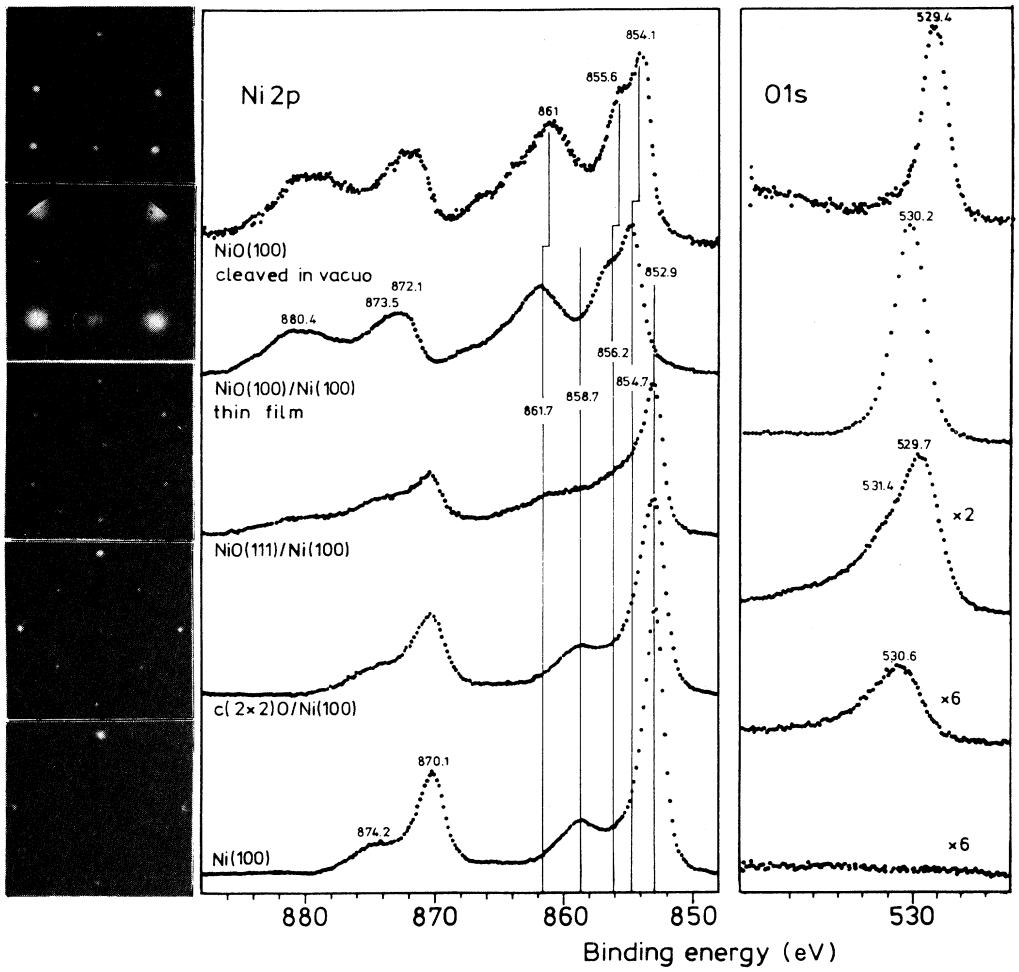

FIG. 1. Ni $2p$ and O $1s$ XP spectra and the corresponding LEED patterns for a NiO(100) single crystal cleaved *in vacuo* and a Ni(100) surface treated with different oxygen doses.

consider the generally accepted but debatable view that NiO is an ionic solid built from Ni^{2+} cations and O^{2-} anions arranged in a rock-salt structure. The data suggest that oxygen is in an anionic state in both the adsorbates as well as in the oxide while for Ni to become cationic all metal-metal interactions have to be detached as is the case in the oxide. The formation of Ni^{2+} is accompanied by a change in the electron configuration from $3d^9 4s^1$ in the metal to $3d^8$ in the oxide. Based on the $3d^8$ ground-state configuration of Ni^{2+} there have been many attempts to assign the Ni $2p$ core-hole spectra.[31] The main point to remember in this connection is the localization of the core hole and of the $3d$ valence orbitals, and connected with this the high gain in energy via screening these localized states by electrons from neighboring atoms. The screening in the case of NiO leads to a configuration $2p^5 3d^9 L^{-1}$ for the core-hole state of lowest energy, i.e., a configuration where a ligand electron from the oxygen atoms has been transferred towards the Ni atom to screen the Ni core hole. The unscreened configuration of the core ionized Ni^{2+} is $2p^5 3d^8$. Both these electron configurations lead to a manifold of electronic terms that determine the spectra function of the core ionization. Detailed calculations have been carried out on this problem[31] and several authors agree that this is the appropriate description of the experimental observations. A more detailed assignment of the various features in the spectrum may be taken from the literature.[31] This assignment reveals that the two features at low binding energy basically result from the $2p^5 3d^9 L^{-1}$ configuration while the peak at higher binding energy originates from the $2p^5 3d^8$ configuration. Additional fine structure is due to multiplet splitting.[31] As revealed in Fig. 1 the splittings and intensities are very similar for the NiO film and the bulk sample which indicates that the splitting is not due to defects (Ni^{3+}) as suggested in the literature.[32] However, it is worthwhile to note that for the valence ionizations a conceptually very similar assignment has been proposed as for the core ionizations. But this is still a matter of debate in the literature[33,34] and we come back to this in Sec. III A 2.

Another result of this section is a rough estimate of the thickness of the oxide layer: As revealed in Fig. 1 the Ni $2p$ peak of the substrate is not to be seen in the spectrum of the NiO film. From this we conclude that the thickness of the NiO film is greater than the escape depth of the electrons at this energy, giving us as an estimate a thickness of at least 4–5 layers of NiO on top of the metallic Ni substrate. This is in line with previous studies on the growth of NiO(100) layers on top of Ni(100) under comparable conditions.[6,13,35]

2. *ARUPS data*

We have estimated on the basis of the XPS data a thickness of the oxide film of 4–5 monolayers, and the question is whether the finite thickness manifests itself in the electronic band structure of the oxide film in particular in a direction in k space that corresponds to a direction in real space perpendicular to the surface plane. The right side of Fig. 2 shows a schematic representation of the Brillouin zone of NiO and its relation to the (100) surface Brillouin zone and the left panel shows the NiO(100) structure in direct comparison with the Ni(100) metal surface. Experimentally it is easy to probe the [100] direction by varying the photon energy at normal emission. Figure 3 shows a set of NiO(100) spectra taken from differently prepared NiO(100) surfaces with photon energies close to 21 eV. Shown at the bottom [spectrum (a)] is a spectrum of bulk NiO(100) cleaved *in vacuo* and in order to avoid charging heated to $T=500$ K. Spectrum (b) is from a bulk NiO sample *ex vacuo* cut and polished. The spectrum at the top [spectrum (c)] is due to a thin film of NiO(100) grown on a Ni(100) surface. The spectra show several features which shall be discussed in the following before we analyze the photon-energy dependences.

There are five features below the Fermi energy in spec-

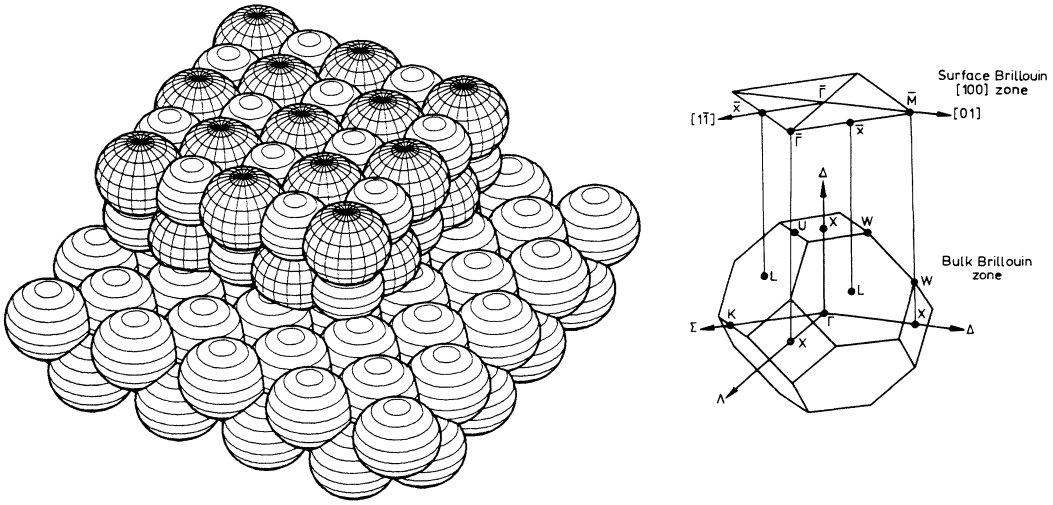

FIG. 2. Left panel: Structure plot for a NiO(100) cluster on a Ni(100) surface. This plot should only be regarded as a model. Right panel: Bulk Brillouin zone and corresponding (100) surface Brillouin zone for Ni and NiO (fcc). Reproduced from Ref. 36.

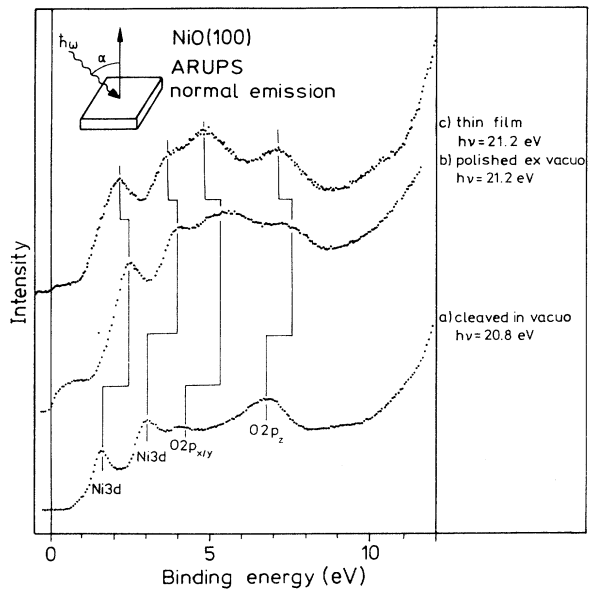

FIG. 3. Normal-emission ARUPS valence-band spectra for differently prepared NiO(100) surfaces. The angles of light incidence are 32.5°, 32.5°, and 45° for spectra (a), (b), and (c), respectively.

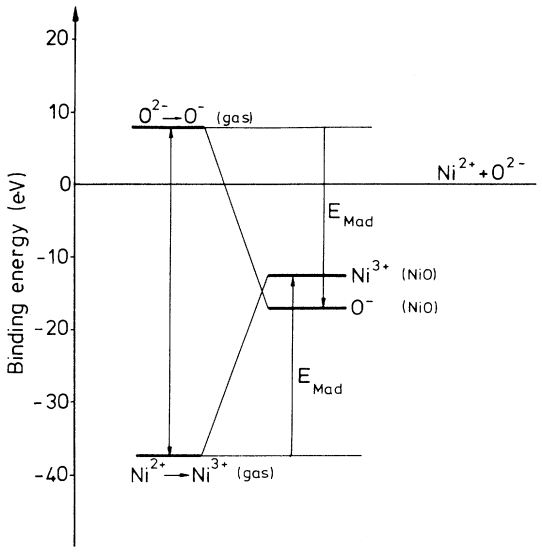

FIG. 4. Energy-level diagram comparing the binding energies of the first Ni^{2+} and O^{2-} valence ionizations for isolated ions and NiO. E_{Mad} is the Madelung energy which is 24 eV in the NiO bulk and 23 eV on the NiO(100) surface.

trum (c) taken with 21 eV photon energy: 2.2, 3.6, 4.8, 7.1 eV, and a weak emission close to the Fermi edge. The peak close to the Fermi energy which does not appear in spectrum (a) and is considerably stronger in spectrum (b) is probably due to defect emission within the gap or to emission from the underlying substrate in the case of the thin oxide film. Connected with this, all peaks are shifted to lower (higher) binding energies in spectra (a) and (b). We shall come back to this point later.

The two features at 2.2 and 3.6 eV are due to Ni *d* band emission, while the features at 4.8 and 7.1 eV are due to emission from the oxygen 2*p* bands. If we adopt the accepted view that NiO must be considered as an ionic crystal built from Ni^{2+} and O^{2-} ions it appears somewhat strange that the 3*d* emission from the positively charged Ni ions is situated at lower binding energy as compared to the negatively charged oxygen ions. However, this can be explained in a straightforward manner by considering the free-ion energies together with the Madelung energy of NiO (24 eV).[37] The scheme shown in Fig. 4 qualitatively explains the energetic ordering of the Ni and O valence states in the photoemission spectra. Energies are given relative to the free-ion energies of Ni^{2+} and O^{2-}. Ionization of Ni^{2+} takes 36.16 eV according to Ref. 38, while removal of an electron from O^{2-} is accompanied by an energy gain of 6.5 eV.[39] If we assume that both ions experience the same Madelung potential with different signs then the Madelung energy destabilizes the Ni^{3+} level by 24 eV and stabilizes the O^- level by the same amount. Consequently, the binding energy of an electron from Ni^{2+} is less than that from O^{2-}. This is also the case for the NiO(100) surface since the surface Madelung energy is only slightly different from the bulk Madelung energy (23 eV).[37] While these simple considerations explain the sequence of valence ionizations qualitatively it is obvious that the absolute values are off by about 6 eV even if we consider the work function of NiO of 4.3 eV.[40] In order to further explain the observed number of peaks in the valence photoelectron spectrum we first have to consider the ligand field splitting of the ionic levels. For Ni^{2+} this yields a t_{2g} and an e_g level at Γ which split in the $\Gamma-X$ direction perpendicular to the surface into b/e and a/b representations, respectively. For O^{2-} we expect one level (t_{1u}) at Γ to split into an *e* and an *a* level along $\Gamma-X$. We neglect in this discussion the fact that NiO is an antiferromagnetic material.

Starting from the energy positions of the isolated ions interatomic interactions have to be included. Based on the general knowledge that the Ni 3*d* valence electrons are localized to a large extent we do not expect strong Ni-Ni interactions, while Ni-O and in particular O-O interactions are important due to the lower degree of radial contraction of the oxygen valence 2*p* electrons. Ni-O interaction only comes into play via hybridization and it is known from cluster calculations that there is hybridization to some extent.[34] To first order we therefore expect little band dispersions for the Ni bands, but pronounced band dispersions for the oxygen bands.

On the basis of these simple considerations we are in a position to try to understand the measured dispersion curves which refer to a direction perpendicular to the surface. Figures 5(a) and 5(b) show two sets of spectra as a function of photon energy for NiO(100)/Ni(100) and for bulk NiO(100). We have plotted the measured binding energies of the oxide film as a function of photon energies as *E* versus $k_{[100]}$ dispersions in Fig. 6(a) and compare these values with those determined for bulk NiO shown in Fig. 6(b). For both the NiO film and the bulk sample we used an inner potential of 3.5 eV which was deter-

mined by the zero slope method[41] and an effective mass of $m^*=m_e$. For a band structure of cleaved NiO(100) recently published by Shen *et al.*[8] the authors used an inner potential of 8 eV and an effective mass of $m^*=0.95m_e$. When we apply these parameters to our ARUPS data, we find that the O $2p_z$ band which reappears in the spectra at photon energies of about 55 eV [open circles in Fig. 6(b)] does not match the O $2p_z$ band seen at photon energies of about 20 eV [solid circles in Fig. 6(b)]. We could avoid this problem by using an effective mass of $m^*=0.9m_e$ but at kinetic energies of about 50 eV and higher an effective mass of $m^*=m_e$ seems to be the more appropriate choice since in this energy range the electrons behave more or less free-electron-like. The authors of the paper mentioned above could not see the O $2p_z$ band at 55 eV since they used a Seya-Namioka monochromator and were not able to use photon energies higher than 35 eV.

By comparison of the band structures shown in Figs. 6(a) and 6(b) we find that on a phenomenological basis, except for some details, the NiO film exhibits characteristics comparable with bulk NiO. That this is so in a direction in **k** space perpendicular to the surface even though we are dealing with a film only some layers thick is important for the present study but also represents an interesting result in itself. The dispersion curves obtained from the measurements along the surface plane which are not shown are also very similar to those obtained for a bulk sample. This, however, is not too surprising because we can expect periodicity parallel to the surface in the two-dimensional layer. How sensitive these dispersions are towards the existence of defects in the layer is basically unknown, and the present ARUPS results provide no further clues in this direction. It appears that the observed larger widths of the peaks in the thin oxide layers are due to the presence of defects as scattering centers for the escaping electrons.

At Γ the three oxygen $2p$ levels are degenerate in the

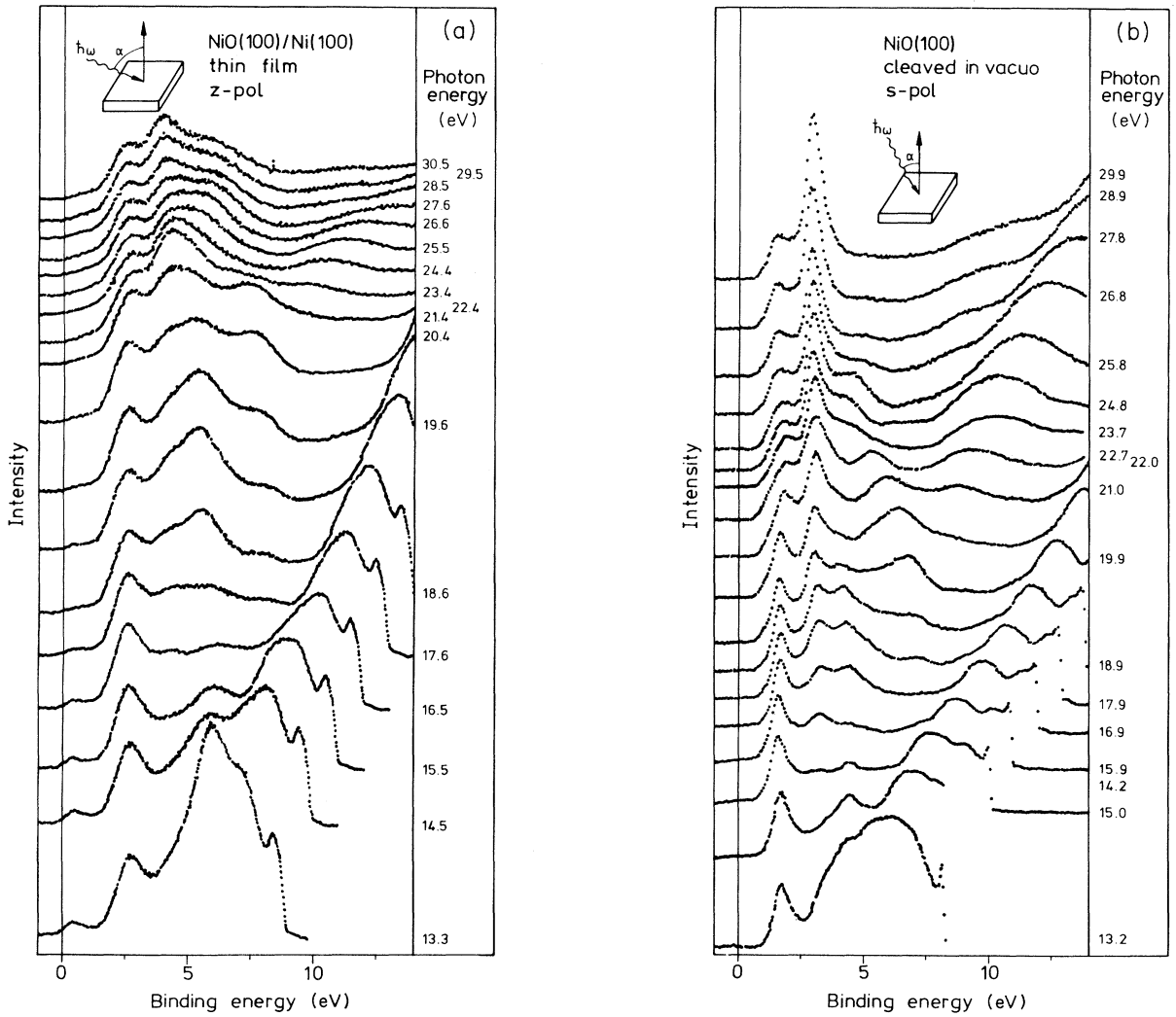

FIG. 5. Series of normal-emission ARUPS valence-band spectra. Panel (a): NiO(100) film grown on Ni(100), $\alpha=70°$. Panel (b): Cleaved NiO(100) single-crystal surface, $\alpha=32.5°$.

cubic environment of the NiO lattice. Along the $\Gamma-X$ direction within the Brillouin zone the levels split into a nondegenerate O $2p_z$-derived band and a doubly degenerate O $2p_{x,y}$-derived band. To find out the character of the bands we used the polarization dependence of the photoemission features as shown in Fig. 7. The O $2p_z$ band should exhibit characteristic attenuation of the emission intensity when the light polarization is changed from z to xy (s) polarization. Figure 7 compares spectra taken with mainly s- and mainly z-polarized light for the bulk oxide and the oxidized Ni(100) sample. At photon energies of 56.7 and 21.3 eV, respectively, we probe a momentum vector near the middle of the $\Gamma-X$ line where the oxygen levels are split as just discussed. Inspection of Fig. 7 allows us to clearly identify the band at about 6-eV binding energy as the oxygen-induced O $2p_z$ band. The next highest band is mainly due to the O $2p_{x,y}$-derived bands which exhibit a smaller dispersion. For the Ni bands experimentally there is no clearly detectable dispersion. The reason for this behavior of the Ni ionizations has been discussed in the literature by several groups[11,19,22,42,43] and it is connected with the fact that electron correlation and, in particular hole localization have to be considered. In our view Fujimori and Minami[34] and Janssen and Nieuwport[33] have presented the most satisfactory theoretical calculations on this problem up to now. They describe the electronic states of the neutral ground state and ionized NiO within a configuration-interaction cluster calculation. Briefly, they find as expected a Ni $3d^8$ configuration to be the ground-state configuration of the NiO_6^{10-} cluster. The ionized NiO_6^{9-} is described by considering configuration interaction between $3d^7$, $3d^8L^{-1}$, and $3d^9L^{-2}$ configurations, i.e., it cannot be satisfactorily described by a single configuration. Each configuration leads to a manifold of multiplet terms. The situation is very similar to the one encountered with the Ni $2p$ core ionizations. The two most important configurations are the unscreened $3d^7$ and the oxygen screened $3d^8L^{-1}$ configurations. These configurations lead to multiplet terms $^4T_1$, $^2T_1$ and ^2E, which are spread in energy over a range of 10 eV. A graphical representation of the result of Fujimori and Minami is shown in Fig. 8.[34] The most intense lines are situated at the valence-band edge, about

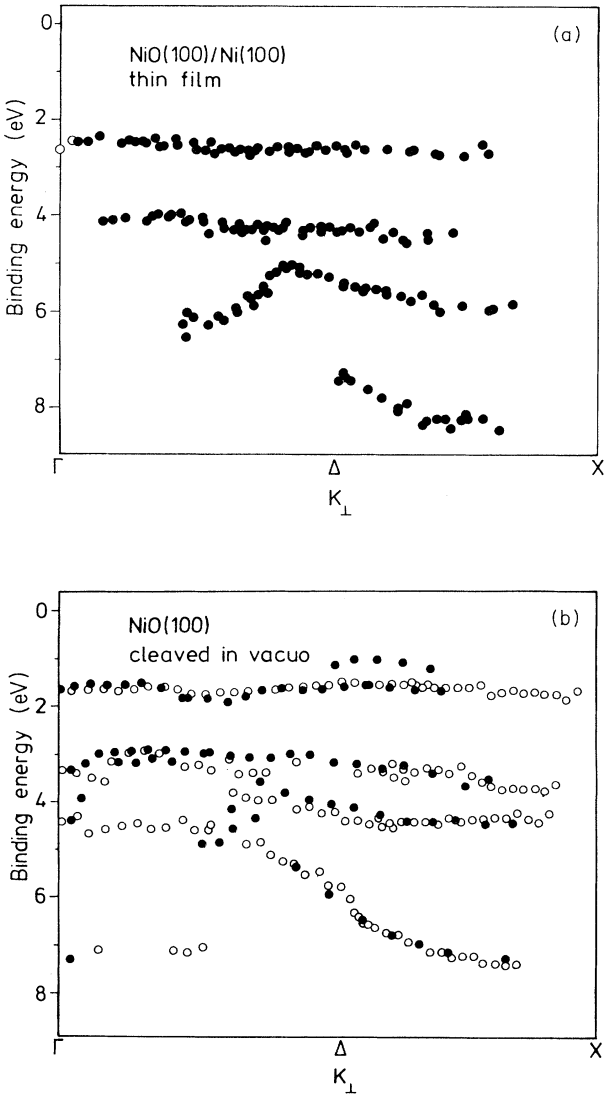

FIG. 6. Experimentally determined valence-band structure for NiO(100)/Ni(100) [panel (a)] and *in vacuo* cleaved NiO(100) [panel (b)]. Solid circles represent data points in the first half of the second Brillouin zone, whereas open circles are data points folded back from the second half of the second Brillouin zone.

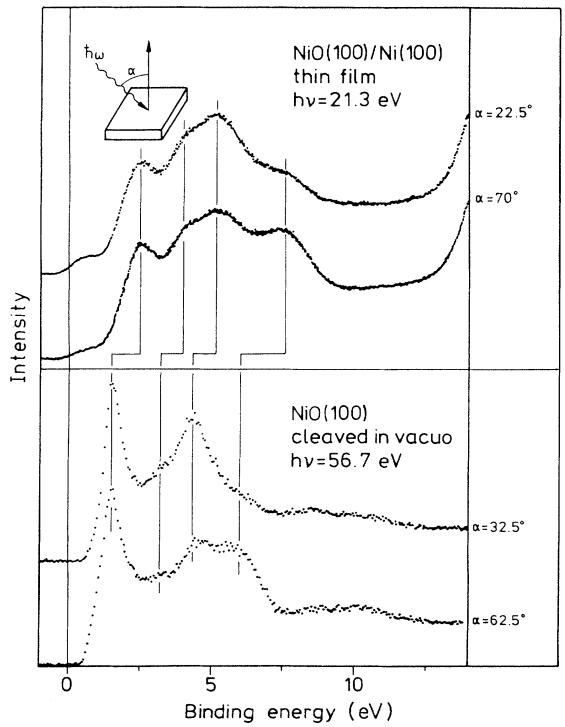

FIG. 7. Comparison of valence-band ARUP spectra taken with differently polarized light for a cleaved NiO(100) sample and a thin NiO(100) film.

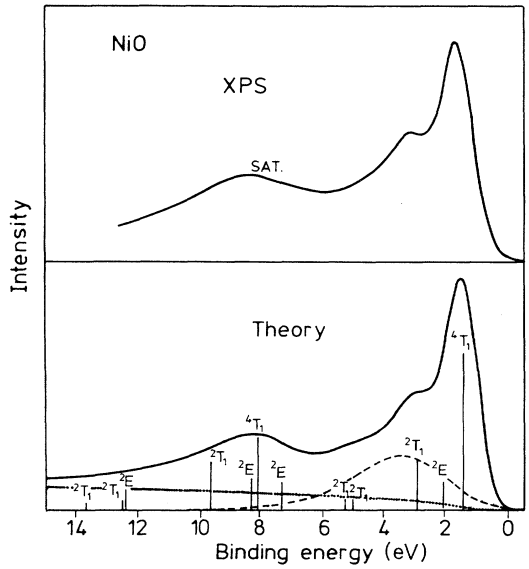

FIG. 8. Theoretical assignment of the Ni valence-band ionizations of NiO as reproduced from Ref. 34.

2 eV below, and between 7–10 eV. The two low-energy features are dominated by the $3d^8L^{-1}$ configuration according to Fujimori and Minami[34] while the feature at high binding energy is dominated by the $3d^7$ configuration. It should be noted, however, that the mixing is substantial and strong configuration mixing has to be considered for all peaks. In other words, all Ni-induced peaks are part of one spectral function. In order to investigate the different contributions of the Ni- and O-derived levels to the spectral function we investigated the photon-energy dependence of the photoemission features. The photon-energy dependences of the photoionization cross section of Ni 3*d* versus O 2*p* levels which are plotted in Fig. 9 as taken from Yeh and Lindau[44] show that at 20 eV O 2*p* dominates while already at 50 eV Ni 3*d* has an equivalent cross section. At higher photon energies the Ni 3*d* levels get more and more dominant. Of course, this has consequences for the dispersion

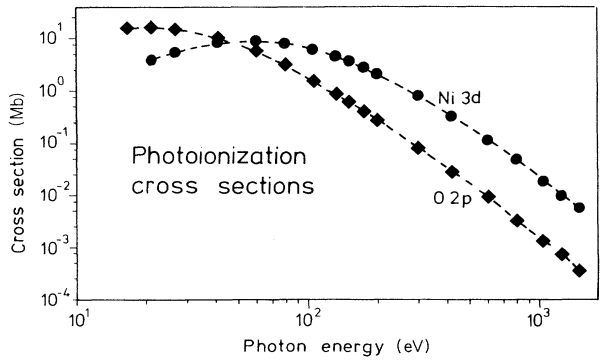

FIG. 9. Photoionization cross sections of the Ni 3*d* ($3d^8$) and the O 2*p* ($2p^6$) levels as a function of photon energy. Data have been taken from Ref. 44.

measurements plotted in Fig. 6: in order to determine the oxygen band dispersions it is advantageous to use low photon energies where the oxygen cross section dominates the Ni 3*d* cross section. At higher photon energies it is likely that one of the many Ni 3*d*-induced states is more intense than the oxygen-induced features. This happens, indeed, for the peak close to 7-eV binding energy with respect to the Fermi energy. At low photon energy we see in Fig. 6(b) the dispersion of the O $2p_z$ level towards lower binding energy approaching Γ (solid circles). As we move towards higher photon energies leaving the first Brillouin zone we find in the first half of the second Brillouin zone a feature close to 7-eV binding energy that does not show pronounced dispersions. We believe that this is due to another Ni 3*d* satellite, i.e., another multiplet term (see Fig. 8). The dominance of the Ni 3*d* peaks becomes even more pronounced when we sweep the photon energy through the Ni 3*p* and Ni 3*s* thresholds as shown in Figs. 10(a) and 10(b). For comparison we have included valence-band XP spectra where the O 2*p* emission is nearly totally suppressed. Between 64 and 66 eV several features in the photoelectron spectrum of the valence electron region resonate. This has been observed earlier by Thuler, Benbow, and Hurych[45] and by Oh *et al.*[46] and has been traced back to resonance photoemission involving an excitation of the Ni 3*p* electron into an unoccupied Ni 3*d* state which subsequently autoionizes and yields a satellite final state. The 3*p*-3*d* transition is allowed if we assume atomiclike transitions, and it remains allowed, of course, if we reduce the symmetry to the octahedral point group of NiO. For the 3*s* threshold the situation is more complicated and has not been discussed previously. Figure 10(b) shows very similar resonance behavior as compared with the Ni 3*p* threshold. However, on an atomic basis a 3*s*-3*d* transition is forbidden. It remains forbidden even after reduction of symmetry as long as we do not allow for Ni 3*d*–O 2*p* mixing. We know from our NEXAFS data, which are discussed below, that there is some Ni-O hybridization and this could cause the resonances near the Ni 3*s* threshold.

We may therefore state that for the description of the electronic structure of NiO the oxygen sublattice may be approximately described in a band-structure picture while the Ni sublattice cannot be described in a band structure picture due to the rather high degree of localization of the electrons on the Ni sites. If there is Ni-O hybridization then it is quite plausible that this hybridization leads to partial transfer of the relatively large oxygen dispersion into the Ni bands.

At this point we come back to the discussion of the emission close to the Fermi energy found in the cases of NiO(100)/Ni(100) and the polished NiO(100) sample (see Fig. 3). In both cases all NiO-induced features are shifted to larger binding energies indicating the existence of defect states in the band gap which are different from the defect states of bulk NiO. The defect states pin the Fermi energy within the gap which is known to be about 4.3 eV wide in NiO.[47] Therefore, the defect states are located closer to the conduction band than to the valence band for the oxide layer and polished NiO, which means that they are donor defects in contrast to the situation for

bulk NiO which is a p-type semiconductor.[30] Based on such considerations the emission near the Fermi energy could probably be emission from defect states. In order to analyze the nature of this feature we have plotted the intensity of this emission relative to the intensity of the NiO d-band emission as a function of photon energy as shown in Fig. 11(a). Obviously the photon-energy dependence of the cross section is such that the emission near to the Fermi edge must be due to Ni d states. If this feature was due to O $2p$ emission we would expect a strong decrease with increase photon energy as indicated by the solid line in Fig. 11(a). The observed behavior fits much better to the intensity variations of Ni states. This interpretation is corroborated by the results shown in Fig. 11(b). Here we plotted the $k_{[100]}$ dispersions of the emissions at the Fermi edge in comparison with the valence-band dispersions for clean Ni(100). Clearly the dispersions observed for both the thin NiO(100) layer and the polished NiO(100) sample are similar to the valence-band dispersions of the clean Ni(100) surface. We tend to attribute the feature near to the Fermi edge in the case of NiO(100)/Ni(100) at least partly to emission from the underlying Ni(100) surface. This interpretation is supported by the LEED pattern observed from the oxidized sample used for the ARUPS measurements since we could see dimly the LEED spots of the underlying substrate. Thus the oxide layer was thin enough to allow electrons from the substrate to travel through the oxide film. For the

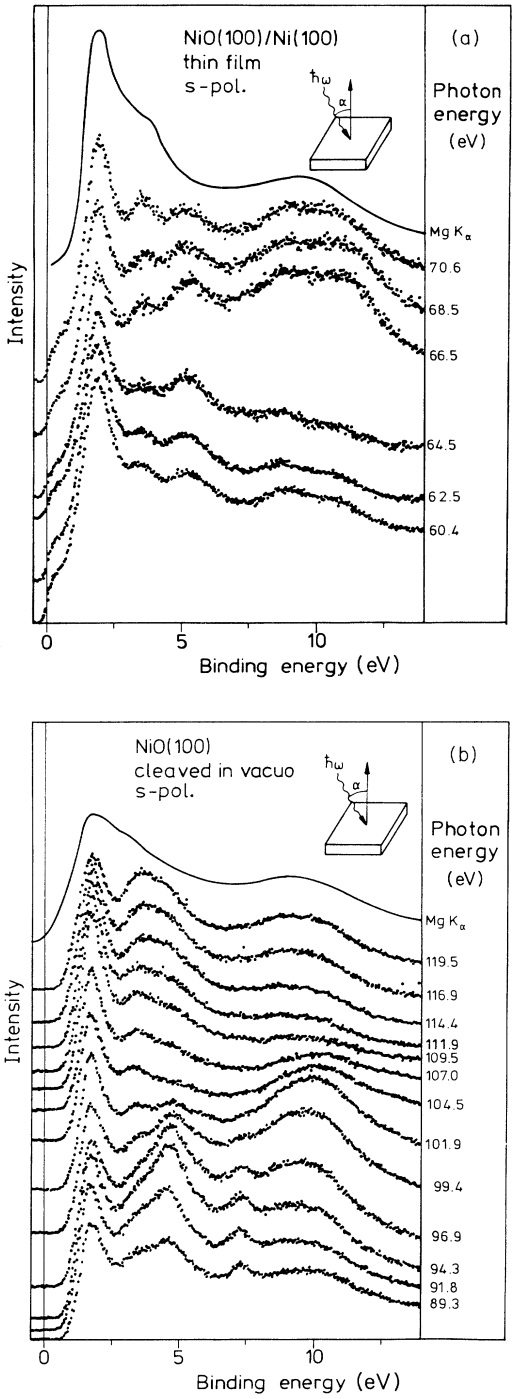

FIG. 10. Series of ARUP valence-band spectra in normal emission for photon energies in the range of the Ni $3p$ [panel (a)] and the Ni $3s$ threshold [panel (b)]. In both cases the angle of light incidence was 32.5°. For comparison in both cases a valence-band XP spectrum is shown. The XP spectrum in panel (a) has been taken from Ref. 9.

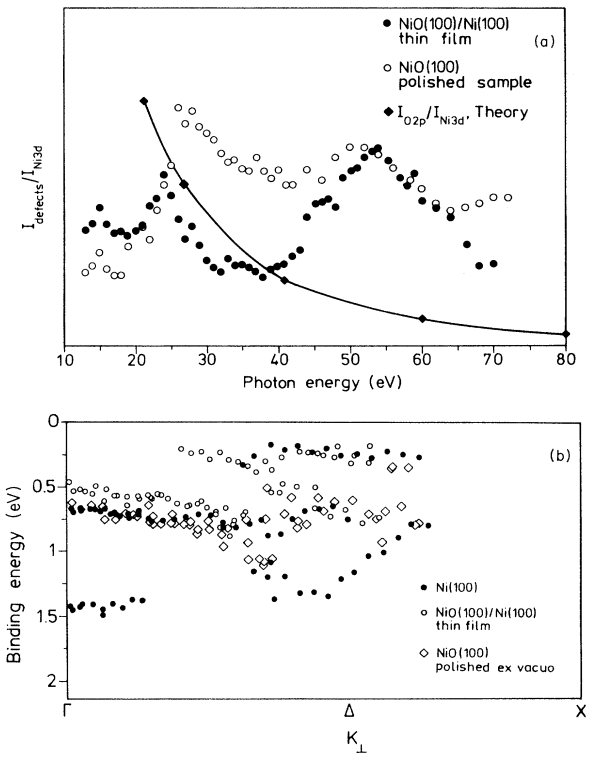

FIG. 11. Panel (a): Photoemission intensity of the emission near the Fermi edge for NiO(100)/Ni(100) and a NiO(100) single-crystal sample polished *ex vacuo*. The data for the calculated curve have been taken from Ref. 44. Panel (b): Dispersions of the valence bands of a Ni(100) surface as a function of k_{100} in comparison with the dispersions observed for the emissions near E_F for a thin NiO(100) film and for a polished NiO(100) single-crystal sample.

polished sample we know from AES that the surface stoichiometry [Ni]:[O] is about 2:1. In this context we interpret the feature near the Fermi edge in the case of the polished sample to originate from metallic clusters large enough to develop a Ni(100)-like valence-band structure. Such metallic clusters have been observed previously on a polished NiO(100) sample with reflection high-energy electron diffraction (RHEED) by Korte and Meyer-Ehmsen[48] and for chemically reduced NiO(100) by Floquet and Dufour.[49]

3. *NEXAFS data*

Figure 12 shows an oxygen K-edge NEXAF spectrum of the NiO(100) film. The relative intensities of the features do not vary as a function of the angle of photon incidence. We show this spectrum to demonstrate that there is no difference to a corresponding spectrum of bulk NiO which has been published before. Sawatzky *et al.*[50] have given an assignment of the observed features. According to them the isolated peak at lowest excitation energy is connected with an excitation of an O 1s electron into the Ni d shell to form a O $1s^{-1}3d^9$ configuration. It appears reasonable and has been discussed in this way by Sawatzky *et al.* to take the relatively high cross section of this excitation as a hint in favor of considerable Ni-O hybridization. All other peaks are noncharacteristic in that they seem to be observed in oxides in general, i.e., those oxides that have no d electrons.[51] The similarity of the spectra taken on the film with those from bulk NiO demonstrate that not only the occupied electron states but also the unoccupied states of the film are comparable with those of bulk NiO.

4. *HREELS results*

The evolution of an oxide layer on top of the metallic substrate can be followed in Fig. 13 on the basis of HREEL spectra. Figure 13 shows a series of HREEL spectra that correspond to NiO films with varying average thicknesses. In addition, HREELS spectra of the $p(2\times2)$ and the $c(2\times2)$ adsorbates have been included. The spectra of these adsorbates on the metallic substrates have been discussed in detail by Tahman *et al.*,[52] Szeftel *et al.*,[53] and Franchy, Wuttig, and Ibach[54] and we shall not repeat this discussion here. We merely use these spectra to show how we can monitor the appearance of the oxide structure by the appearance of the very strong surface phonons with a principal loss frequency of 620 cm^{-1}. Very similar spectra have been reported previously by Dalmai-Imelik, Bertolini, and Rousseau.[4] These surface phonons are of Fuchs-Kliewer type, and the usual assumption is that they should change their frequency as a function of the thickness of the oxide layer.[55] (In the case of NiO we estimate a variation of the phonon loss energy due to dispersion to be of the order of a few meV.) However, this is not necessarily valid if the layer is bound to a metal on one side and to the vacuum on the other which is the case for the thin oxide film.[56] Accordingly we could not detect any shift in the phonon frequency with varying thickness of the oxide layer. The losses at higher energies in the oxide spectra are due to multiple-scattering events. As expected for such processes the loss intensities decrease according to a Poisson distribution. This is shown in the inset of Fig. 13.

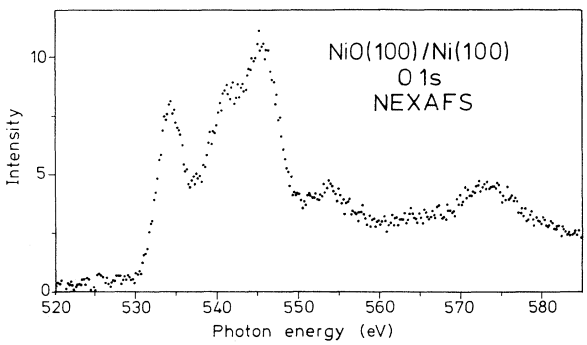

FIG. 12. O 1s NEXAF spectrum of NiO(100)/Ni(100).

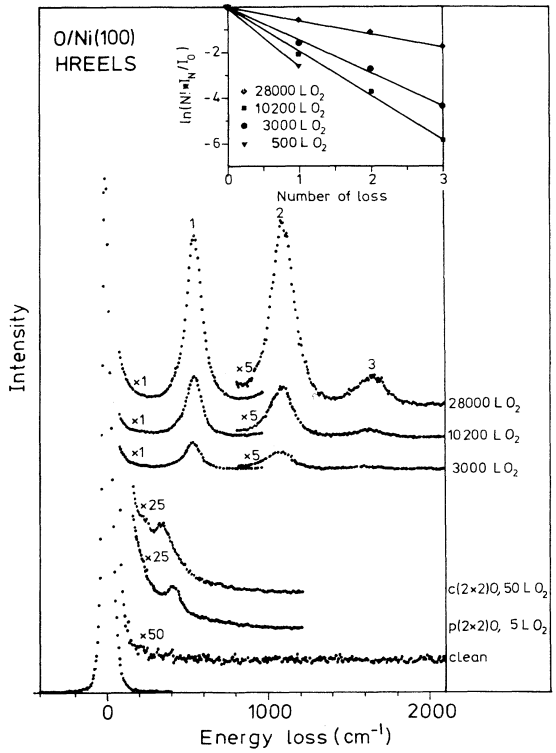

FIG. 13. Series of HREEL spectra obtained for different oxygen exposures on Ni(100). The inset shows the Poisson distributions of the intensities of the Fuchs-Kliewer phonon losses for some oxide layers of different thicknesses.

B. NO adsorption on NiO

1. *Thermal-desorption data*

Figure 14 shows the thermal-desorption spectra of NO from a bulk NiO(100) surface in comparison with desorption from the oxide layer. The desorption temperatures for both systems are only marginally different. If we con-

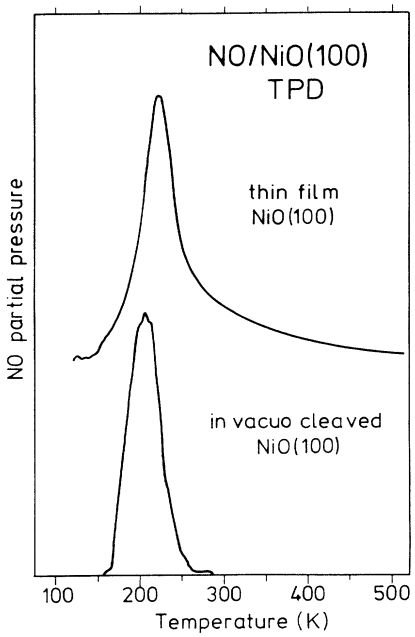

FIG. 14. Comparison of thermal-desorption spectra for NO adsorbed on a NiO(100) film and NO adsorbed on a cleaved NiO(100) single-crystal sample.

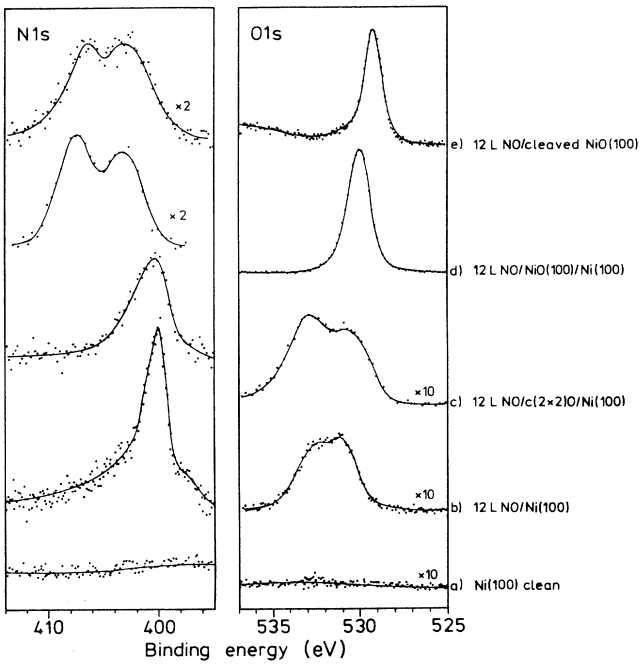

FIG. 15. Set of N 1*s* and O 1*s* XP spectra for NO adsorbed on different substrates.

sider the different heating rates and identical, commonly used frequency factors we calculate on the basis of the Readhead formula almost identical desorption energies for both cases, i.e., 0.52 eV. This means that NO is weakly chemisorbed on a NiO surface. It is quite surprising that the desorption energies on both surfaces are the same because the defect densities are different by orders of magnitude as judged from the LEED spots, and one is tempted to expect a strong influence of the defects on the desorption temperature. However, even though we do not know the exact nature of the defects the similarity of the desorption temperatures indicates that the defects are not the sites of NO adsorption on the oxide film.

In order to quantify the NO coverage on the NiO surface, which is important to judge whether we are dealing with defect adsorption or not, it is very problematic to use TDS data because the NiO data cannot be referenced to NO adsorption data on the clean Ni(100) surface. NO dissociates in the desorption process on clean Ni(100) while it does not dissociate during the desorption process from NiO.[17,19–22,57] We therefore refer to XPS data, which shall be discussed in the Sec. III B 2, where these problems do not occur. Before we discuss the XPS data it is worthwhile to compare the desorption temperatures of NO on the oxide surface with those on the clean and chemisorbed oxygen covered metal surfaces: For NO desorbing from clean Ni(100) the peak temperature is $T=350$ K, for $c(2\times2)$O precovered Ni(100) it is $T=420$ K.[17,19–22] It appears that the bonding towards the metal surface, i.e., with the presence of metallic Ni-Ni interactions and a Ni electron configuration close to $3d^9 4s^1$, is considerably stronger than on the oxide surface where direct Ni-Ni interactions are much weaker and the electron configuration on the Ni ions is $3d^8$. We shall discuss in the final section a simple molecular-orbital (MO) picture that allows us to understand the bonding on the oxide surface.

2. *XPS data*

There are two aspects of the XPS data that we discuss in this section: (a) the determination of NO coverage on NiO(100) and (b) the line shape of the N 1*s* NO signal of the adsorbed species.

Figure 15 shows a set of XP spectra. The left panel shows N 1*s* spectra and the right panel shows O 1*s* spectra. At the bottom [spectra (a)] the signals from the clean surface are shown. Spectra (b) show the signals from NO on the clean Ni(100) surface. The left spectrum exhibits a slightly asymmetric N 1*s* peak very similar to the spectrum reported earlier by Shen *et al.*[58] The splitting of the O 1*s* feature results from the coexistence of several adsorbed NO species[59] in bent and upright coordinations on different adsorption sites as revealed by HREELS.[19,22] Spectra (c) are spectra of an oxygen precovered surface exposed subsequently to NO. We have used the $c(2\times2)$ LEED pattern of the oxygen precovered surface to calibrate the O 1*s* signal if we assume that the $c(2\times2)$ pattern corresponds to a coverage of $\theta=0.5$. We can use the O 1*s* signal to calibrate the N 1*s* signal from the NO covered surface. With this procedure we know the size of a N 1*s* signal that corresponds to a NO coverage of $\theta=0.5$ with respect to the number of Ni atoms in the first layer. The N 1*s* signal of the coadsorbate is slightly shifted and exhibits a larger width than the signal from the clean surface. We have reason to believe that this is due to the overlap of several signals originating from different chemical species which have been identified earlier by

TABLE I. N 1*s* and O 1*s* binding energies for gaseous NO and NO adsorbed on different substrates. Gas-phase data have been taken from Ref. 69. The N 1*s* binding energy for gas-phase NO is the weighted average of two different spin configurations.

	N 1*s*		O 1*s*	
NO/Ni(100)	400.1		532.4	531.0
NO/c(2×2)O/Ni(100)	401.0		532.9	
NO/NiO(100) epitaxial	407.5	403.1		
NO/NiO(100) cleaved	407.2	402.8		
NO gas phase	406.4		539.2	

HREELS[19–22] and observed with monochromatized XPS.[59]

Clearly, as we turn to the spectrum of NO adsorbed on the thin-film-oxide surface the habit of the N 1*s* spectrum [spectrum (d)] changes quite dramatically. The O 1*s* spectrum of the adsorbed layer cannot be differentiated from the dominant oxide signal. The N 1*s* spectrum shows two well-separated peaks which are both at considerably higher binding energies as compared with the adsorbates on the metallic surface. Table I collects the measured binding energies with respect to the Fermi level of the metallic Ni substrate. Using the calibration discussed above for the N 1*s* signal area we are now in the position to determine the total nitrogen coverage on the NiO layer. Since on the perfect NiO surface the number of available Ni sites is reduced by 25% as compared to the metallic Ni surface we determine a coverage of $\theta=0.2$. Considering the relatively high defect density on the oxidized Ni(100) surface this coverage value may be compatible with adsorption at defect sites. However, the N 1*s* peak of NO on the perfect *in vacuo* cleaved NiO surface shown in spectrum (e) is similar to the one of NO on the oxide film and the coverage is also nearly the same as estimated by the signal-to-background ratio of the N 1*s* signal. The widths of the individual lines for the bulk sample are slightly larger than those for the thin oxide film and the relative intensities also seem not be the same, but we attribute this to the statistics of the data and to the deliberately diminished resolution of the electron analyzer chosen in the latter case. This was necessary because the spectra were taken with high angular resolution so that at high energy resolution the count rate would have been untolerably low. Apart from this the spectra are identical. Since the coverage is similar to the case of the oxide layer and the defect density is much lower we can only conclude that the species are not defect bound.

The next problem is the interpretaion of the N 1*s* double-peak spectrum of NO on the NiO surface. The natural explanation would be the existence of two chemically different species. However, if this were the case we would expect changes of the relative intensities of the two peaks as the concentration of the species changes. Although a change in surface temperature or the exposure to laser light[20,21] changes the coverage of NO a variation of the relative intensities has never been observed. The most conclusive experimental observation as to the nonexistence of several chemical species is provided via the HREELS measurements presented in Sec. III B 3. It turns out that there is only one NO bond-stretching frequency observed in the spectrum, so that we have within the given resolution of our experiment only conclusive evidence for one chemical species. On the other hand, if this is the case, then there is only one possible explanation, which, as we shall show in the following, is a quite natural one, namely the existence of very intense satellite structure. While for metal surfaces it is quite well known that in the case of weak molecular chemisorption systems such as CO/Cu, CO/Ag, CO/Au, N_2/Ni, and N_2/Ru,[60–66] "giant" satellite structures are rather the rule than the exception. Such satellite structures have not been observed for adsorbates on insulator or semiconductor surfaces. Considering, however, that intense satellite structure is well known also for molecular compounds with rather extended π-electron systems, such as paranitroanniline and related compounds with high electron polarizabilities,[67,68] the proposed explanation is not at all surprising. In fact, we shall show in the following that the observed binding energies (see Table I) can be explained in a straightforward manner by considering a simple screening model: We know from the gas phase how much energy is necessary to create a N 1*s* hole in NO.[69] Disregarding the fact that the N 1*s* peak of NO is exchange split due to the two possible final triplet and singlet states,[69] the average N 1*s* binding energy with respect to the Fermi energy (work function=4.3 eV) is 406.4 eV (Ref. 69) which is very close to the peak of adsorbed NO at highest binding energy. We can now calculate the energy released via a screening of this core hole by transferring an electron from the substrate to the lowest unoccupied level of adsorbed NO. This is done in a gedankenexperiment where we first take an electron out of the substrate to infinity, and then bring the electron back to the core-ionized NO molecule. Because it has been shown that the valence electron structure of a core-ionized species is very well described via the so-called equivalent core model,[70,71] the electron affinity of a N 1*s* ionized NO is equal to the first ionization potential of O_2 ($I_p=12$ eV).[72] Since the latter energy is well defined it is the question how much energy is necessary to take an electron out of the surface into a region of space that overlaps with the NO molecule. This is the important point which makes the difference with respect to the situation at a metal surface. While at a metal surface it is a good approximation to consider the work function as the minimum energy to take an electron out at any place on the surface, this is not the case on a semiconductor or insulator surface. The energy necessary to take an electron out of a semiconductor is the sum of the work function, which may be dependent on the place of electron detachment, and the energy needed to take one electron from

the highest occupied electronic level to the Fermi edge. This sum is about 7 eV in the case of NiO. Since the electron affinity we have to consider in our case is still larger than the energy necessary to take an electron out of the substrate, an energy of about 5 eV is still gained by transfering an electron towards the core-ionized molecule. Therefore, this screened state should have a binding energy about 5 eV lower than the gas-phase value referenced to the Fermi level. This is very close to the observed second peak in the adsorbate spectrum. The reason for the equal intensities of the peaks lies in the coupling strength between molecule and substrate. While for strong coupling we would expect the screened peak to be dominant, the unscreened peak would be most intense in the case of very weak coupling.[62,73–75] Weak chemisorption represents the case of intermediate coupling where both peaks exhibit almost equal intensity.[62,73–75] The consequences of the various couplings on the spectral functions in adsorbate systems have been discussed by several authors and we refer to the literature for details.[62,73–75] We can check whether the above argument concerning the Fermi level is correct by referring to the spectra of the NO adsorbates on the metal surface. In this case, the work function is the appropriate energy necessary for release of an electron. This would then place the screened level with respect to the oxide surface at about 2 eV even lower binding energy. Figure 15 shows that this is close to the experimental observations. Also, on the metal surface the coupling is strong, and therefore we observe only very small satellite intensity. Summarizing, we feel that the presented assignments provide us with a proper interpretation of the XP data of NO on the NiO surface in terms of giant shake-up satellites.

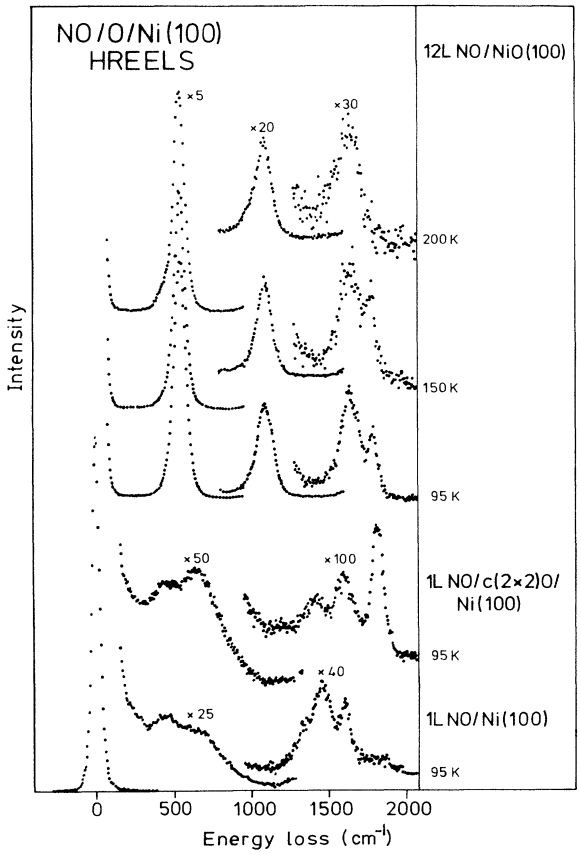

FIG. 16. Series of HREEL spectra obtained for NO adsorbed clean Ni(100), oxygen precovered Ni(100), and NiO(100) grown on Ni(100) at different temperatures.

3. *HREELS data*

Figure 16 shows some HREEL spectra of NO on a NiO(100) film at different temperatures. Upon exposure to NO at low temperature, we observe in addition to the very strong NiO surface phonons addressed above (see Sec. III A 4) one peak at the high-frequency side of the third multiple-phonon loss. This peak vanishes at about 200 K surface temperature in agreement with the thermal-desorption data which showed a peak temperature only a little above $T=200$ K. We assign this peak to the N=O bond-stretching vibration of NO adsorbed on top of Ni sites in the NiO layer. This assignment is based on a detailed HREELS study of NO-oxygen coadsorption on Ni(100) published earlier.[19,22] We have plotted HREELS spectra of NO on Ni(100) and NO+O on Ni(100) for comparison in Fig. 16. Both spectra are rather complex, and a detailed discussion shows that the spectra are caused by the superposition of a set of different species.[19,22] The important aspect for the present purpose is the appearance of a single peak at 1800 cm^{-1} for adsorption near coadsorbed oxygen. This peak has been assigned to NO adsorbed on top of Ni atoms with a bent Ni-NO bond. The bending of the axis in the coadsorbate is also indicated by the appearance of a bending vibration at 640 cm^{-1}, typical for a strongly bound system.[76] We have transferred this assignment to the oxide surface although we do not observe a bending mode. We cannot exclude at present that such a bending vibration is situated near the position of the NiO phonon loss but this would imply that the force constant of the bending mode on the oxide surface is similar to the adsorbate on the metal surface. However, we know that the molecule substrate bonding is much weaker on the oxide surface as compared with the metal surface, so that we expect a reduced bending force constant. This would shift the bending mode to lower frequencies which might render the bending mode unobservable under the present conditions. Clearly, an independent experimental clue as to the geometry of the molcular axis is highly desirable. We have therefore performed NEXAFS investigations on the NO/NiO(100) adsorbate.

4. *NEXAFS data*

For the NiO(100) film on the Ni(100) surface we have performed a N K-edge NEXAFS study on the NO saturated surface. These data are shown in Fig. 17. We compare two spectra at normal incidence and at grazing incidence. The narrow peaks at low photon energy are due to the N $1s-2\pi$ resonance which may be excited with

the light polarization vector oriented perpendicular to the molecular axis. The broader bands at higher photon energies are due to the so-called σ shape resonance which is polarized along the molecular axis. In other words, for an orientation of the molecular axis perpendicular to the surface plane the NEXAFS signal at normal incidence and perfect polarization would only consist of the π resonance. Therefore, if we monitor the variation of the relative intensities of σ and π resonances as a function of the light incidence angle we may deduce the angle between the molecular axis and the surface normal. Kordesch *et al.*[77] have developed an equation to determine the polar orientation of the molecular axis with respect to the surface normal where a random azimuthal orientation of the molecular axis is assumed,

$$\frac{I_\sigma}{I_\pi} = K \frac{P(\sin^2\vartheta\sin^2\theta + 2\cos^2\vartheta\cos^2\theta) + (1-P)\sin^2\vartheta}{1 - P\cos^2\theta}, \tag{1}$$

where K is a proportionality constant, ϑ is the tilt angle; and θ is the angle of incidence. In this equation the Fresnel formulas that determine the amount of parallel and perpendicular polarized light with respect to the surface have been neglected. Only the degree of polarization P of the monochromatized synchrotron light has been incorporated into the equation. In order to take the Fresnel equations into account we should know the optical constants of the material in question for the particular photon energies. In general, and in particular in our case the optical constants are not available and we have to rely on the original equation. Figure 17 shows the experimental data together with calculated curves according to Eq. (1) where the angle between the molecular axis and the surface normal is the parameter. In comparison with our data gained on the oxide surface we have also plotted as open circles the experimental data taken for NO on clean Ni(100) and on NO+O on Ni(100). The problem in this comparison is that between the metallic surface and the oxide surface the optical constants may change considerably. Therefore it is problematic to deduce the tilting angle with a high degree of accuracy. We feel, however, that the conclusion of a tilted geometry with a tilt angle higher than 20° with respect to the surface normal is certainly justified. The directly deduced angle of 45° may be too large. Our NEXAFS data thus provide independent evidence for a tilted geometry of the NO adsorbate on the oxide surface.

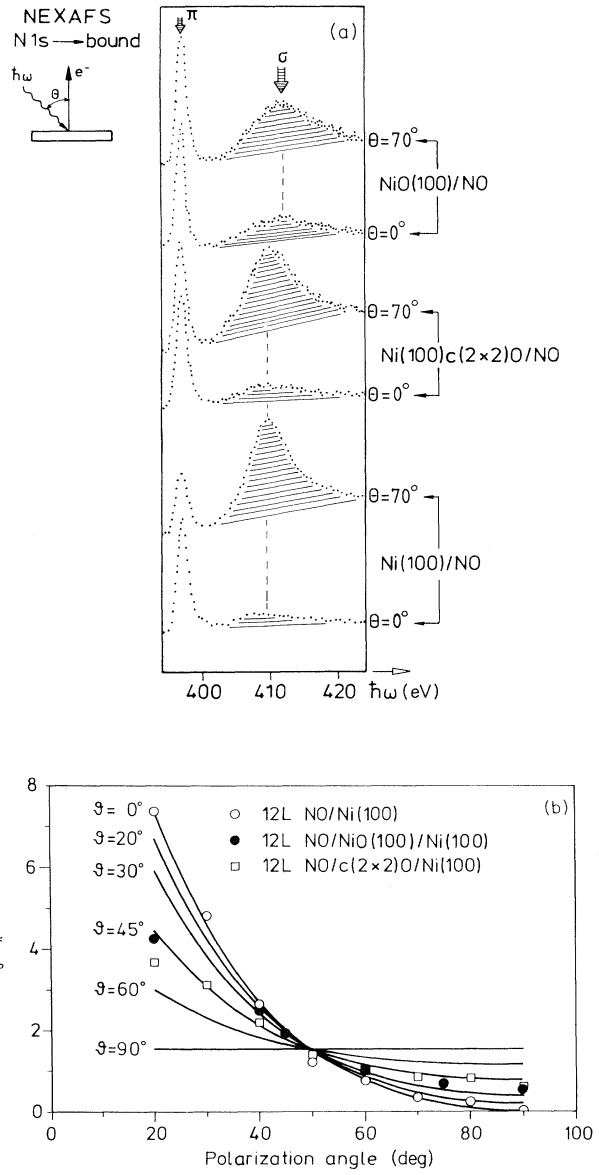

FIG. 17. N 1*s* NEXAFS results for NO adsorbed on NiO(100)/Ni(100) in comparison with results for NO adsorbed on Ni(100) and $c(2\times2)$O/Ni(100). Panel (a): N 1*s* NEXAF spectra for perpendicular and grazing light incidence. Panel (b): Experimentally determined σ/π intensity ratios as a function of the light incidence angle together with calculated curves for different molecular orientations of the adsorbed NO molecules.

5. *Cluster calculations: The bonding of NO on NiO*

We have shown that NO weakly chemisorbs on NiO on regular Ni sites with the molecular axis bent with respect to the surface normal. This may be explained on the basis of *ab initio* cluster calculations on a NiO_5 cluster with one NO molecule bound N-end towards the Ni atom. In Fig. 18 the results are presented in a simplifying one-electron picture. For a perpendicularly oriented NO molecule the relevant part of the MO scheme may be represented as shown in the left part of Fig. 18: the Ni 3*d* levels are split into a set of three closely spaced fully occupied orbitals remnant of the t_{2g} orbitals in octahedral NiO_6, and an only slightly split subset of two singly occupied Ni 3*d* orbitals remnant of the e_g orbitals in octahedral NiO_6. Above the Ni levels the singly occupied NO 2π orbital is situated. The three unpaired electrons may be coupled to form quartet and doublet states. The ground state turns out to be the quartet state. NO 2π and Ni orbitals transform according to different irreducible representations of the C_{4v} point group as indicated in Fig. 18. Consequently, the bonding interaction is very

Orbital	$d_{x^2-y^2}$	d_{z^2}	π_x	π_y	
NO linear	b_1	a_1	e	e	c_{4v}
NO tilted	a'	a'	a'	a''	c_s
	a	a	a	a	c_1

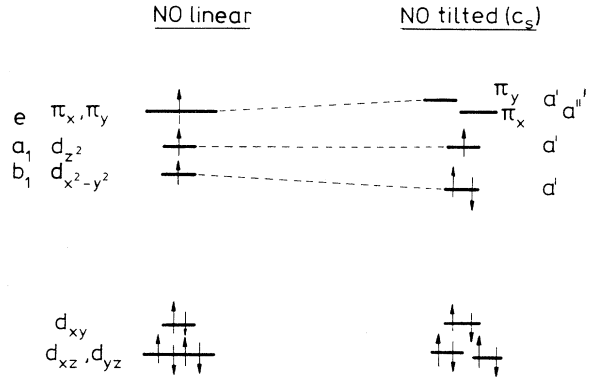

FIG. 18. One-electron scheme of the Ni $3d$ and NO 2π levels for NO adsorbed on NiO(100) in a linear and a bent configuration.

weak if there is any at all. However, if the NO molecular axis is tilted the symmetry is reduced, and the irreducible representations change. Now, one component of the NO 2π transforms according to the same irreducible representation as the Ni $3d$ levels and there will be mixing, i.e., formation of bonding and antibonding orbitals. This leads to a stabilization of the lowest Ni $3d$ level. If this level is doubly occupied the system gains energy and is stabilized. Thus, in this simple one-electron scheme a bent configuration is the stable arrangement.

On this problem *ab initio* calculations have been performed. For the electronic ground state of the linearly coordinated NO—NiO_5 cluster self-consistent-field (SCF) calculations corrected for the basis-set superposition error (BSSE) and followed by a configuration-interaction (CI) calculation, including Ni $3d$ and NO 2π orbitals, yield an energy slightly above zero, i.e., no bonding. The basis set consisted of double ζ (DZ) functions as listed in Table II. To test this result also SCF calculations using basis functions of triple ζ quality with polarization (TZP) functions, also corrected for the BSSE, were performed on this cluster. The result differed only slightly in energy from the result of the first calculation but now a potential minimum was found with a binding energy of 0.04 eV. The basis set for the latter calculation is also listed in Table II. The ground state of the first calculation consists by more than 98% of the $3d^8 4s^0$ configuration similar to the ground state Janssen and Nieuwpoort[33] calculated for a NiO_6^{10-} cluster.

The calculations for the NO-NiO_5 cluster with the NO molecule tilted along the Ni-O direction of the NiO_5 cluster were performed using the same procedure as in the first calculation, i.e., SCF calculations using DZ basis functions followed by a CI calculation including Ni $3d$ and NO 2π orbitals. Due to the reduced symmetry of the cluster now also charge-transfer configurations of the Ni $3d$ and NO 2π orbitals have to be taken into account. Referred to the ground-state energy of the first calculation we got a potential minimum of -0.17 eV for a NO tilting angle of about 45°. The electronic valence state at this angle mainly consists of the charge-transfer configurations

$$[(\text{“}t_{2g}\text{”})^6(d_{z^2})^1(d_{x^2-y^2})^2(\pi_x)^0] ,$$

$$[(\text{“}t_{2g}\text{”})^6(d_{z^2})^2(d_{x^2-y^2})^1(\pi_x)^0] ,$$

$$[(\text{“}t_{2g}\text{”})^6(d_{z^2})^0(d_{x^2-y^2})^1(\pi_x)^2] ,$$

$$[(\text{“}t_{2g}\text{”})^6(d_{z^2})^1(d_{x^2-y^2})^0(\pi_x)^2] ,$$

with CI coefficients ranging from 0.45 to 0.53, indicating that not only the one configuration shown in the right part of Fig. 18 contributes to the ground-state wave function but also other configurations; two of them with doubly occupied 2π orbitals are important. The binding energies for some electronic states of the NO-NiO_5 cluster as a function of the NO tilting angle are shown in Fig. 19. All data points have been calculated for a Ni-N spacing of 2.1 Å.

Electronic states of NiO with partial occupation of the Ni $4s$ orbital are shifted to higher energy as compared to the Ni metal because of the quasioctahedral environment of strongly repulsive O atoms and the adsorbate. In order to prove that this is also valid for the NO-NiO_5 cluster we enlarged the CI space, including the lone-pair NO 5σ and the Ni $4s$ orbital. We got the result that electronic states involving the Ni $4s$ orbital are found at energies more than 1 eV above those states which are essential to

TABLE II. Basis sets used for the SCF and CI calculations for the NO-NiO_5 cluster. Numbers in square brackets denote the contraction of the wave functions. The notation $7s,3p[4,2]$, for instance, means that seven s and three p functions have been contracted to four s functions and two p functions.

	DZ	TZP
Ni[a]	$13s,6p,4d[9,4,3]$	$13s,6p,4d[9,4,3]+1f(2.0)$
O (NO)[b]	$7s,3p[4,2]$	$9s,5p[6,3]+1d(1.25)$
N[b]	$7s,3p[4,2]$	$9s,5p[6,3]+1d(0.9)$
O (NiO)[b]	$7s,3p[4,2]$	$7s,3p[4,2]$

[a]Reference 79.
[b]Reference 80.

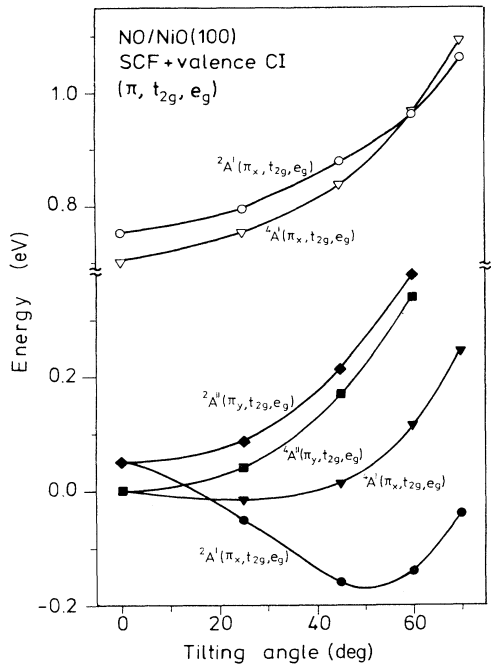

FIG. 19. Calculated energies of a NO-NiO_5 cluster for some electronic states as a function of the tilting angle of the NO molecule. Energies are referenced to the ground state of NO adsorbed in a linear configuration.

explain the NO-NiO interaction. So far we have not taken any N-Ni interactions or any Ni $3d^9L^{-1}$ configurations into account. This is justified since both contributions are small where the Ni $3d^9L^{-1}$ configurations represent the larger contribution as has been shown by Fujimori and Minami.[34] The most severe approximation within these calculation may be neglect of NO-O backbonding interactions in the CI calculations.

The behavior of higher electronic states of $^4A'$ and $^2A'$ symmetry is also shown in Fig. 19. The splitting between the first and the second $^4A'$ and $^2A'$ states is due to the large exchange integral between the $d_{x^2-y^2}$ and the d_{z^2} orbitals (0.8–1.0 eV), whereas the splitting within the first $^{4,2}A'$ states and the second $^{4,2}A'$ states is much less pronounced because the exchange integrals involve orbitals located on different centers (Ni $3d$, NO 2π). Apart from this, excited electronic states like $(t_{2g})^5(e_g)^3$ or $(t_{2g})^5(e_g)^2(2\pi)^1$ are energetically separated from $(t_{2g})^6(e_g)^2$ by more than 0.8 eV. The details of the calculations will be published elsewhere.[78]

IV. CONCLUSIONS

We have investigated the electronic properties of a thin NiO(100) film in comparison with data for a NiO(100) single crystal surface and the adsorption of NO on these surfaces. In both cases NO is found to adsorb on regular NiO adsorption sites and not on defect sites with a desorption temperature of about 220 K. CO adsorption could not be observed down to temperatures of about 90 K under UHV conditions. Our findings are in line with those reported by Escalona Platero, Coluccia, and Zecchina.[14] The NO bond-stretching frequency that these authors extrapolate for the ideal NiO(100) surface is especially in perfect agreement with the results of the present study. In conclusion we may state that the observed tilted bonding geometry of NO on the NiO surface may be quantitatively understood on the basis of simple considerations and verified using high-quality *ab initio* calculations.[78] A complementary paper dealing with the structural properties of NiO(100)/Ni(100) as investigated by STM and SPA-LEED will be published elsewhere.[7]

ACKNOWLEDGMENTS

This work has been funded by the German Federal Minister for Research and Technology (BMFT) under Contract No. 05 327 AAB and the Deutsche Forschungsgemeinschaft. We thank Professor W. Mönch for supplying us with construction plans for a crystal-cleaving tool. Dr. W. Braun (BESSY GmbH) and Dr. R. Reininger (HASYLAB Synchrotron Radiation Center) are gratefully acknowledged for technical assistance.

[1]V. E. Henrich, Rep. Prog. Phys. **48**, 1481 (1985).
[2]G. Heiland and H. Lüth, in *The Chemical Physics of Solid Surfaces and Heterogeneous Catalysis*, edited by D. A. King and D. P. Woodruff (Elsevier, New York, 1982), Vol. 3, Chap. 4.
[3]K. Wandelt, Surf. Sci. Rep. **2**, 1 (1982).
[4]G. Dalmai-Imelik, J. C. Bertolini, and J. Rousseau, Surf. Sci. **63**, 67 (1977).
[5]H. Conrad, G. Ertl, J. Küppers, and E. E. Latta, Solid State Commun. **17**, 497 (1975).
[6]R. S. Saiki, A. P. Kaduwela, J. Osterwalder, C. S. Fadley, and C. R. Brundle, Phys. Rev. B **40**, 1586 (1989).
[7]M. Bäumer, D. Cappus, H. Kuhlenbeck, H.-J. Freund, G. Wilhelmi, A. Brodde, and H. Neddermeyer (unpublished).
[8]Z.-X. Shen, C. K. Shih, O. Jepsen, W. E. Spicer, I. Lindau, and J. W. Allen, Phys. Rev. Lett. **64**, 2442 (1990).
[9]S. Hüfner and G. Wertheim, Phys. Rev. B **8**, 4857 (1973).
[10]S. Hüfner, F. Hullinger, J. Osterwalder, and T. Riesterer, Solid State Commun. **50**, 83 (1984).
[11]S. Hüfner, J. Osterwalder, T. Riesterer, and F. Hullinger, Solid State Commmun. **52**, 793 (1984).
[12]G. Wertheim and S. Hüfner, Phys. Rev. Lett. **28**, 1028 (1972).
[13]W.-D. Wang, N. J. Wu, and P. A. Thiel, J. Chem. Phys. **92**, 2025 (1990).
[14]E. Escalona Platero, S. Coluccia, and A. Zecchina, Langmuir **1**, 407 (1985); M. W. Roberts and R. S. Smart, Surf. Sci. **100**, 590 (1980); G.-M. Schwab and J. Block, Z. Phys. Chem. **1**, 42 (1954); M. E. Dry and F. S. Stone, Discuss. Faraday Soc. **28**, 192 (1959); E.-G. Schlosser, Ber. Bunsenges. **71**, 352 (1967).
[15]A. Boudriss and L. C. Dufour, in *New Stoichiometric Compounds Surfaces, Grain Boundaries and Structural Defects*, edited by J. Nowotny and W. Weppner (Kluwer Academic, Amsterdam, 1989), pp. 311–320.

[16]R. P. Furstenau and H. A. Langell, Surf. Sci. **159**, 108 (1985).
[17]P. M. Ferm, F. Budde, A. V. Hamza, S. Jakubith, G. Ertl, D. Weide, P. Andresen, and H.-J. Freund, Surf. Sci. **128**, 467 (1989).
[18]D. Fargues and J. J. Ehrhardt, Surf. Sci. **209**, 401 (1989).
[19]G. Odörfer, R. Jaeger, G. Illing, H. Kuhlenbeck, and H.-J. Freund, Surf. Sci. **233**, 44 (1990).
[20]Th. Mull, M. Menges, B. Baumeister, G. Odörfer, H. Geisler, G. Illing, R. M. Jaeger, H. Kuhlenbeck, H.-J. Freund, D. Weide, U. Schüller, P. Andresen, F. Budde, P. Ferm, V. Hamza, and G. Ertl, Phys. Scr. **41**, 134 (1990).
[21]H. Kuhlenbeck, G. Odörfer, R. Jaeger, C. Xu, T. Mull, B. Baumeister, G. Illing, M. Menges, H.-J. Freund, E. W. Plummer, G. Watson, D. Weide, and P. Andresen, Vacuum **41**, 34 (1990).
[22]G. Odörfer, Ph. D. thesis, Universität Bochum, Germany, 1990.
[23]K. Hauffe and S. R. Morrison, *Adsorption* (De Gruyter, Berlin, 1974).
[24]C. F. Conville, D. P. Woodruff, K. C. Prince, G. Paolucci, V. Chab, M. Surman, and A. M. Bradshaw, Surf. Sci. **168**, 221 (1986); J. Somers, Th. Lindner, M. Surman, A. M. Bradshaw, G. P. Williams, C. F. Conville, and D. P. Woodruff, *ibid.* **183**, 576 (1987).
[25]S. Hüfner and G. K. Wertheim, Phys. Lett. **51A**, 299 (1975).
[26]S. Kowalczyk, Ph.D. thesis, University of California, 1976.
[27]L. A. Feldkamp and L. C. Davis, Phys. Rev. B **22**, 3644 (1980).
[28]P. Holloway and J. B. Hudson, Surf. Sci. **43**, 123 (1974).
[29]U. Starke, P. L. de Andres, D. K. Saldin, K. Heinz, and J. B. Pendry, Phys. Rev. B **38**, 12 277 (1988); S. R. Chubb, P. M. Marcus, K. Heinz, and K. Müller, *ibid.* **41**, 5417 (1990).
[30]N. L. Peterson and C. L. Wiley, J. Chem. Phys. Solids **46**, 43 (1985).
[31]B. Wallbank, I. G. Main, and C. E. Johnson, J. Electron Spectrosc. Relat. Phenom. **5**, 259 (1974); K. S. Kim, *ibid.* **3**, 217 (1974); S. Larsson, Chem. Phys. Lett. **32**, 401 (1975).
[32]M. Tomellini, J. Chem. Soc. Faraday Trans. **84**, 3501 (1988).
[33]G. J. M. Janssen and W. C. Nieuwpoort, Phys. Rev. B **38**, 3449 (1988).
[34]A. Fujimori and F. Minami, Phys. Rev. B **30**, 957 (1984).
[35]P. R. Norton, R. L. Tapping, and J. W. Goodale, Surf. Sci. **65**, 13 (1977).
[36]E. W. Plummer, W. Eberhardt, Adv. Chem. Phys. **49**, 533 (1982).
[37]J. D. Levine and P. Mark, Phys. Rev. **144**, 751 (1966).
[38]C. E. Moore, *Atomic Energy Levels,* Natl. Bur. Stand. (U.S.) Circ. No. 467 (U.S. GPO, Washington, D.C., 1952), Vol. 2.
[39]The value was calculated via a Born-Haber cycle using thermodynamical data from P. W. Atkins, *General Chemistry* (Scientific American, New York, 1989).
[40]This value has been determined from the low-energy cutoff of ARUPS spectra and is in satisfactory agreement with the change of work function upon oxygen exposure as reported in Ref. 28.
[41]M. Wöhlecke, A. Baalmann, and M. Neumann, Solid State Commun. **49**, 217 (1984); A. Baalmann, M. Neumann, W. Braun, and W. Radlik, *ibid.* **54**, 583 (1985).
[42]K. Terakura, A. R. Williams, T. Oguchi, and J. Kübler, Phys. Rev. Lett. **52**, 1830 (1984).
[43]J. M. McKay and V. E. Henrich, Phys. Rev. Lett. **53**, 2343 (1984).
[44]J. J. Yeh and I. Lindau, At. Data Nucl. Data Tables **32**, 1 (1985).
[45]M. R. Thuler, R. L. Benbow, and Z. Hurych, Phys. Rev. B **27**, 2082 (1983).
[46]S.-J- Oh, J. W. Allen, I. Lindau, and J. C. Mikkelsen, Jr., Phys. Rev. B **26**, 4845 (1982).
[47]G. A. Sawatzky and J. W. Allen, Phys. Rev. Lett. **53**, 2339 (1984).
[48]U. Korte and G. Meyer-Ehmsen (unpublished).
[49]N. Floquet and L.-C. Dufour, Surf. Sci. **126**, 543 (1983).
[50]P. Kuiper, G. Kruizinga, J. Ghijsen, and G. A. Sawatzky, Phys. Rev. Lett. **62**, 221 (1989).
[51]S. Nakai, T. Mitsuishi, H. Sugawara, H. Maezawa, T. Matsukawa, S. Mitani, K. Yamasaki, and T. Fujikawa, Phys. Rev. B **36**, 9241 (1987).
[52]T. S. Tahman, D. L. Mills, J. E. Black, J. M. Szeftel, S. Lehwald, and H. Ibach, Phys. Rev. B **30**, 589 (1984).
[53]J. M. Szeftel, S. Lehwald, H. Ibach, T. S. Rahman, J. E. Black, and D. L. Mills, Phys. Rev. Lett. **51**, 268 (1983).
[54]R. Franchy, M. Wuttig, and H. Ibach, Surf. Sci. **215**, 65 (1989).
[55]K. L. Kliewer and R. Fuchs, Adv. Chem. Phys. **27**, 335 (1974).
[56]A. Otto (private communication).
[57]D. E. Peebles, E. L. Hardegree, and J. M. White, Surf. Sci. **148**, 635 (1984).
[58]S. Shen, P. Feulner, E. Umbach, W. Wurth, and D. Menzel, Z. Naturforsch. **42**, 1333 (1987).
[59]A. Nilsson and N. Martensson (private communication).
[60]K. Horn, J. Dinardo, W. Eberhardt, H.-J. Freund, and E. W. Plummer, Surf. Sci. **118**, 465 (1982).
[61]P. R. Norton, R. L. Tapping, and J. W. Goodale, Surf. Sci. **72**, 33 (1978).
[62]H.-J. Freund and E. W. Plummer, Phys. Rev. B **23**, 4859 (1981).
[63]S. Krause, C. Mariani, K. C. Prince, and K. Horn, Surf. Sci. **138**, 305 (1984).
[64]D. Heskett, E. W. Plummer, R. A. de Paola, W. Eberhardt, and F. M. Hoffmann, Surf. Sci. **164**, 490 (1985).
[65]E. Umbach, Solid State Commun. **51**, 365 (1984).
[66]J. C. Fuggle, E. Umbach, D. Menzel, K. Wandelt, and C. R. Brundle, Solid State Commun. **27**, 65 (1978).
[67]H.-J. Freund and R. W. Bigelow, Phys. Scr. **17**, 50 (1987); H.-J. Freund, A. R. Slaughter, S. M. Ballina, M. S. Banna, R. W. Bigelow, B. Dick, J. Lex, and H. M. Deger, J. Chem. Phys. **81**, 2535 (1984).
[68]S. Pignataro and G. Distefano, J. Electron Spectrosc. Relat. Phenom. **2**, 171 (1973); S. Pignataro, R. DiMarino and G. Distefano, *ibid.* **4**, 90 (1974).
[69]K. Siegbahn, C. Nordling, G. Johannson, J. Hedman, P. F. Heden, K. Kamrin, U. Gelius, T. Bergmark, L. O. Werme, R. Manne, and Y. Baer, *ESCA Applied to Free Molecules* (North-Holland, Amsterdam, 1971).
[70]W. L. Jolly and D. N. Hendrickson, J. Am. Chem. Soc. **92**, 1863 (1970).
[71]L. J. Aarons, M. F. Guest, and I. H. Hillier, J. Chem. Soc. Faraday Trans. **68**, 1866 (1972).
[72]D. W. Turner, C. Baker, A. D. Baker, and C. R. Brundle, *Molecular Photoelectron Spectroscopy* (Wiley-Interscience, New York, 1970).
[73]K. Hermann, P. S. Bagus, C. R. Brundle, and D. Menzel, Phys. Rev. B **24**, 7025 (1981).
[74]R. P. Messmer and S. H. Lamson, Chem. Phys. Lett. **65**, 465 (1979).
[75]N. Martensson and A. Nilsson, J. Electron. Spectrosc. Relat. Phenom. **52**, 1 (1990).
[76]L. H. Jones, R. R. Ryan, and L. B. Asprey, J. Chem. Phys. **49**,

581 (1981).
[77]M. E. Kordesch, J. Somers, Th. Lindner, H. Conrad, A. M. Bradshaw, and G. P. Williams, BESSY Annual Report, 1986 (unpublished), p. 223.
[78]M. Pöhlchen and V. Staemmler (unpublished).
[79]B. Roos, A. Veillard, and G. Vinot, Theoret. Chim. Acta **20**, 1 (1971).
[80]S. Huzinaga, J. Chem. Phys. **42**, 1293 (1965).

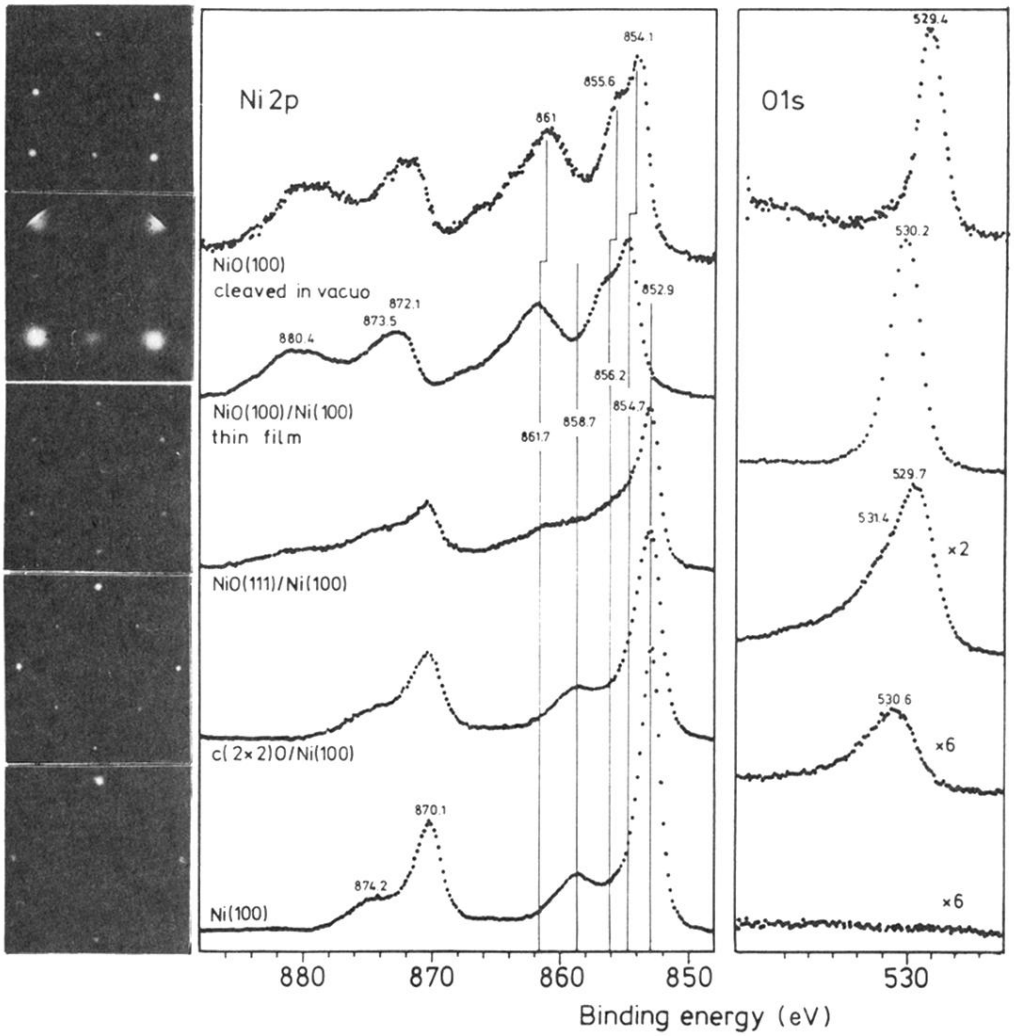

FIG. 1. Ni 2*p* and O 1*s* XP spectra and the corresponding LEED patterns for a NiO(100) single crystal cleaved *in vacuo* and a Ni(100) surface treated with different oxygen doses.